Tesi doctoral presentada per En/Na

Marc PERA TITUS

amb el títol

"Preparation, characterization and modeling of zeolite NaA membranes for the pervaporation dehydration of alcohol mixtures"

per a l'obtenció del títol de Doctor/a en

QUÍMICA

Barcelona, 29 de maig del 2006

Facultat de Química
Departament d'Enginyeria Química

UNIVERSITAT DE BARCELONA

This chapter focuses on the performance of some zeolite NaA membranes synthesized in our laboratory towards the dehydration of alcohol mixtures by VPV. The effect of the operational conditions (feed pressure, permeate pressure, feed composition and temperature) in the performance of the membranes towards the separation of ethanol/water mixtures is shown in section V.1. Moreover, section V.2 describes the performance of the membranes towards the separation of alcohol/water binary mixtures for short and long chain alcohols arising from methanol to 1-pentanol and towards the separation of 1-pentanol/water/DNPE ternary mixture. Finally, section V.3 shows the simulation of a PV zeolite NaA membrane reactor to carry out the liquid-phase etherification reaction of 1-pentanol to di-n-pentyl ether (DNPE) catalyzed by an ion-exchange resin from experimental membrane separation and kinetic data obtained in our laboratory.

V.1. GENERAL TRENDS FOR TOTAL FLUX AND SELECTIVITY TOWARDS DEHYDRATION OF ETHANOL/WATER MIXTURES BY VPV

This section shows the effect of the main operational conditions in the PV process towards the separation of ethanol/water mixtures for good quality zeolite NaA membranes synthesized in this work (see chapter IV). The details concerning the preparation of the membranes and the range of values of the tested operational conditions are summarized, respectively, in Tables V.1 and V.2. All the membranes (zeolite layers: 7-30 μm) displayed low N_2 permeances (~10^{-7} mol m^{-2} s^{-1} Pa^{-1} for membranes ZA1 and ZA2) and (~10^{-9} mol m^{-2} s^{-1} Pa^{-1} for membranes ZA3 – ZA5).

V.1.1. Effect of feed (retentate) pressure

Figure V.1 shows the effect of the feed (retentate) pressure in the range 1-8 bar in the total flux, $\mathbf{N^T}$, and selectivity towards dehydration of an ethanol/water mixture (92 : 8 wt.%) at 323 K by VPV for membranes ZA2 and ZA3. As can be seen, while the total flux tends to rise slightly with the feed pressure, water/ethanol selectivity shows a quite dramatic reduction. Although the membrane shows high quality towards water dehydration, these trends confirm the presence of a reduced number of large non-zeolites pores in the zeolite layer, which might correspond to fissures, cracks or pinholes. In fact, the study of the functional dependence of the total flux and selectivity of a composite zeolite membrane with the feed pressure in a set of VPV experiments might provide valuable data for the quantification and characterization of intercrystalline porosity. In this way, a higher dependence of both properties on the feed pressure might reveal the presence of a higher number of large non-zeolite pores in the zeolite NaA layers. For further insight into this subject see section VI.2.

It should be emphasized that non-zeolite pores, especially the largest ones, might contribute to the PV performance of a membrane even at very low feed pressures, because the permeate vapor is kept at <2 mbar in most of the experiments and a net pressure driving force (at least ~1 bar) exists across the membrane. However, to reduce their contribution, most of the experiments were carried out in this work at a low feed pressure (1.4 – 1.6 bar), but higher than atmospheric pressure to prevent the liquid feed from vaporization at higher temperatures (i.e. 363 K).

Table V.1: Zeolite NaA membranes used in the present study. PV conditions: X_w = 6.67-9.92 wt.%; T=323 K; P_o =1-3 bar; P_v =1-3 mbar

Membrane	*Code (see Table IV.3)*	*Y_W (perm.) (wt.%)*	*$\alpha_{W/E}$ [-]*	*N^T [kg m^{-2} h^{-1}]*
ZA1	**ZA-INN-CF-01**	97.41	502	0.62
ZA2	**ZA-INN-CF-03**	93.35	294	0.39
ZA3	**ZA-INN-SC-18**	99.00	1050	0.49
ZA4	**ZA-INN-C-03**	98.90	1091	0.76
ZA5	**ZA-INN-C-05**	99.84	8538	0.83

Table V.2: Experimental conditions for VPV experiments with ethanol/water mixtures

Feed flow rate [mL min^{-1}]	300
Water feed composition (X_w) [wt.%]	1-60
Temperature (T) [K]	303-363
Feed pressure (P_o) [bar / kPa]	1-8 / 100-800
Permeate vapor pressure (P_v) [mbar / Pa]	1-70 / 100-7000
Stabilization time [h]	2-4
Experimental time [h]	1-3
Number of replicates [-]	2-6

V.1.2. Effect of permeate pressure

Figure V.2 shows the experimental trend of the water flux pervaporated through membrane ZA3 with the permeate vapor pressure. As can be seen, water flux is affected by the vapor permeate pressure, being it reduced with a raise of the permeate vapor pressure. This trend might be explained by the "sweeping" action of vacuum in the permeate, thus allowing

the removal of adsorbed molecules on the permeate/membrane surface. An increase in the permeate vapor pressure might also increase the loading of adsorbed molecules in the membrane/permeate surface, thus reducing the driving force and consequently reducing dramatically the total flux through the membrane.

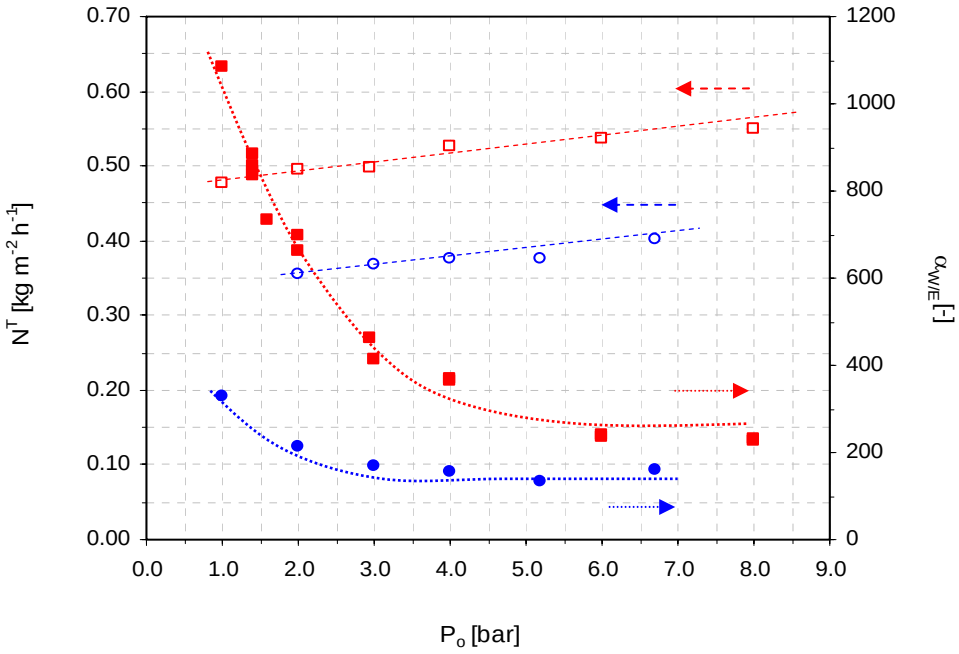

Figure V.1: Evolution of the total flux and selectivity with the feed pressure for the VPV of ethanol/water mixtures. (a) Membrane ZA1 (blue symbols); (b) Membrane ZA3 (red symbols). The void and filled symbols correspond, respectively, to total flux and selectivity. PV conditions: $X_w \approx$ 8.1-9.0 wt.% (x_w = 19.0-20.0 mol%); T=323 K; P_v=1-2 mbar. Standard deviation ≤5% for total flux and ≤10% for selectivity for both membranes. Dashed and dotted lines refer to the trends observed, respectively, for total flux and selectivity.

V.1.3. Effect of feed composition

Figures V.3 shows the effect of the feed composition for the temperature range 303-363 K in the total flux and water/ethanol for the membrane ZA3. As can be seen, the total flux is observed to increase with the water feed composition for all the surveyed temperatures (see Figure V.3a). At low water compositions (20 mol% or <10 wt.%), the total flux shows a linear trend with the water composition, while for values beyond 30-40 mol% (20-30 wt.%), this flux tends to a constant asymptotic value. These observations could be ascribed to the great affinity for water that zeolite NaA shows due to its high hydrophilic character. Thus, the zeolite active layer might preferentially adsorb water over ethanol and as a result, water flux through the

membrane might remain high and constant for high water compositions. On the other hand, the decrease in total flux observed for water compositions <20 mol% could be related to the decrease in the water feed activity. In fact, the trend depicted in Figure V.3a is qualitatively similar to the form of a single-site Langmuir isotherm (see Eq. I.7), which relates surface coverage with partial pressure at equilibrium. This analogy might imply a relevant contribution of water adsorption equilibrium at the liquid feed/membrane surface on the PV performance of the membrane.

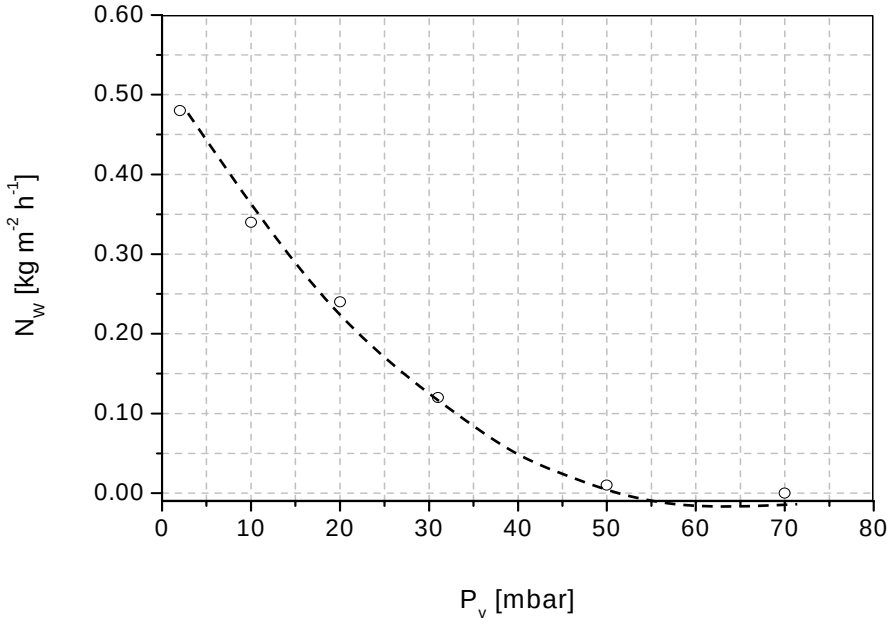

Figure V.2: Evolution of the water flux with the permeate pressure for membrane ZA3. PV conditions: $X_w \approx$ 8.4-9.0 wt.% (x_w = 19.0-20.0 mol%); T=323 K; P_o = 1.4 bar. Standard deviation for water flux <5%. The dashed line refers to the trend observed.

On the other hand, Figure V.3b shows the effect of the feed composition in the selectivity of the membrane for the temperature range under study. As can be seen, the selectivity shows a maximum with the water feed composition in the range 10-20 mol% (5-10 wt.%) in agreement with the results reported by *Okamoto et al. (2001)*, with selectivity values up to 1400 ± 70 at 363 K in the present study. Such high selectivities reflect the great contribution of zeolite pores to discriminate between water and ethanol molecules. However, according to the trends for total flux and selectivity with the feed pressure outlined in Figure V.1, the contribution of non-zeolite domains to total mass transfer cannot be ruled out. The presence of a maximum in the plot of water/ethanol selectivity with the water composition might be explained by the definition of selectivity, $\alpha_{w/E} = [y_w/(1 - y_w)]/[(1 - x_w)/x_w]$. For

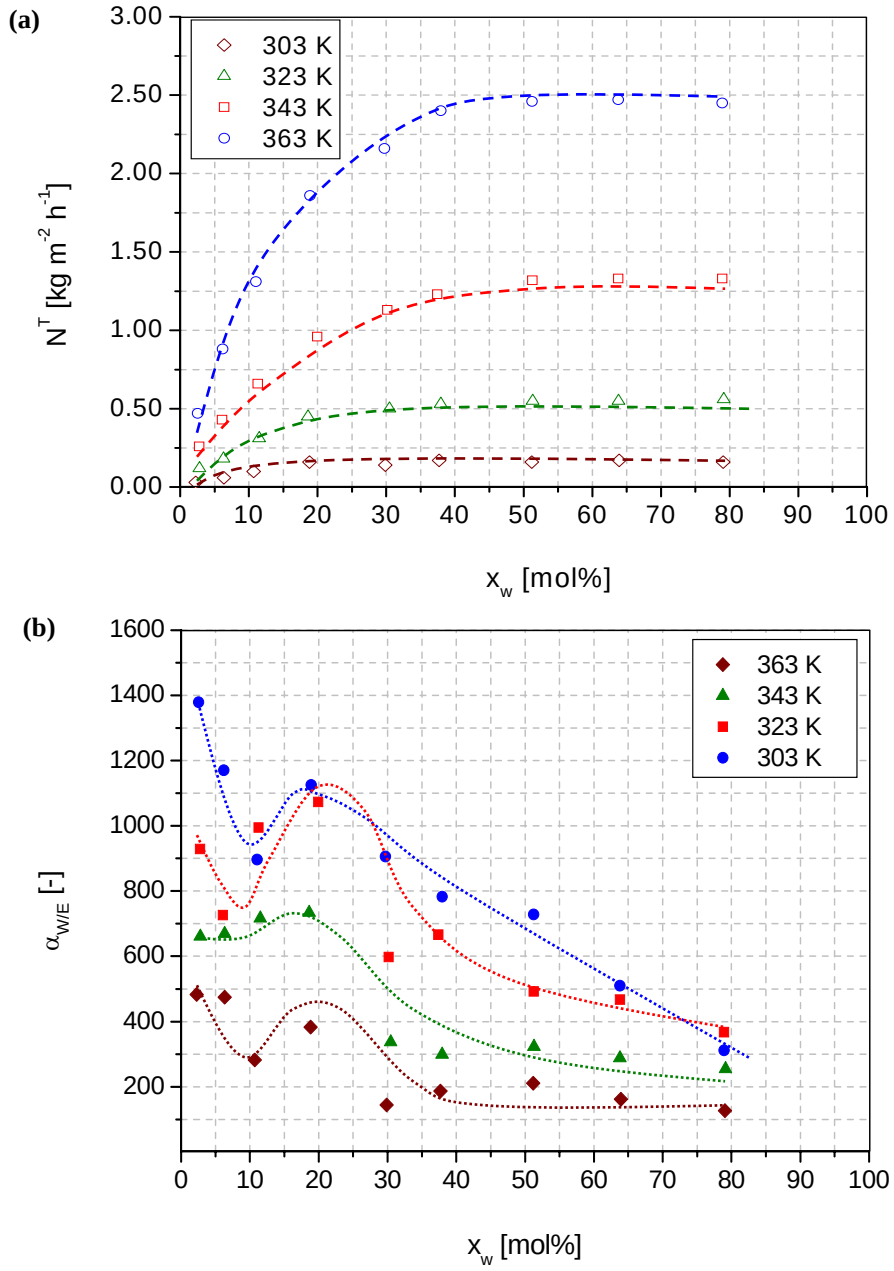

Figure V.3: Evolution of (a) total flux and (b) water/ethanol selectivity with water feed composition (molar) for membrane ZA3. VPV conditions: X_w = 0-100 wt.%, T=303-363 K, P_v = 1 mbar, P_o = 1.6 bar. Standard deviation ≤2% for total flux and ≤4% for selectivity. Dashed and dotted lines refer to the trends observed, respectively, for total flux and selectivity.

water compositions <20 mol% (10 wt.%), water and ethanol fluxes show a dramatic raise, which implies an increase in the selectivity. Otherwise, beyond 20 mol% (10 wt.%), water and ethanol fluxes tend to show a steady value, which involves the reduction of selectivity with water composition according to the function $f(x_w) = [y_w/(1 - y_w)]/[(1 - x_w)/x_w]$.

The trend of the total flux and water/ethanol selectivity with the water feed composition for low water compositions (<20 mol% or 10 wt.%) is plotted in Figure V.4 for membranes ZA1-ZA3 and ZA5. As can be seen, the trend of the total flux with the water composition in the feed (see Figure V.4a) is linear for all the membranes in agreement with the results shown in Figure V.3a. It should be highlighted that membranes ZA1-ZA3 prepared by different seeding and synthesis methods but onto α-Al_2O_3 supports, show linear trends with identical slope. However, the slope for membrane ZA5 synthesized onto TiO_2 (rutile) supports is higher. This difference in the slope of the total flux seems to be in agreement with the trend of the water/ethanol selectivity at low water compositions depicted in Figure V.4b. As can be seen, the water/ethanol selectivity remains practically constant with the water composition for membranes ZA1-ZA3, while for membrane ZA5, the trend is slightly positive. The differences observed for membrane ZA5 and ZA1-ZA3 in the trends of the total flux and the water/ethanol selectivity with the water composition in the feed might be ascribed to a certain role of the support on the PV performance of these membranes.

V.1.4. Effect of temperature

Figures V.5 shows the effect of temperature on the water flux and water/ethanol selectivity of membrane ZA3 for different feed compositions. As can be seen in Figure V.5a, water flux shows values up to 2.50 ± 0.10 kg m^{-2} h^{-1} at 363 K, which are somewhat lower than those reported by *Shah et al. (2000)* and *Okamoto et al. (2001*) and tends to increase with temperature according to an Arrhenius plot, which reveals the activated nature of the permeation process through zeolite crystals. Therefore, Knudsen diffusion, often observed for gas permeation through zeolite A crystals, might be ruled out as the dominating mass transfer mechanism in the current membrane, since a decrease with $T^{-1/2}$ should be expected.

The effective activation energy for water flux, $\mathbf{E^S_{w,eff}}$ [kJ mol^{-1}], computed for this membrane for the system ethanol/water, lies in the range 41-43 kJ mol^{-1} for feed water fractions varying from 6.3-79 mol% (2.5-59 wt.%), which is of the same order as that reported by *Shah et al. (2000)*, 51-52 kJ mol^{-1}, for water feed fractions varying from 22-100 mol% (10-100 wt.%), and 35 kJ mol^{-1} reported by *Okamoto et al. (2001)* for feed water fractions of 22 mol% (10 wt.%) (see Table V.3). Although the effective activation energy remains practically invariable for the range of feed water fractions studied, it should be noted that the intercept of the lines with the ordinate axis at low feed water fractions (i.e. 2.5 wt.%) tends to be lower

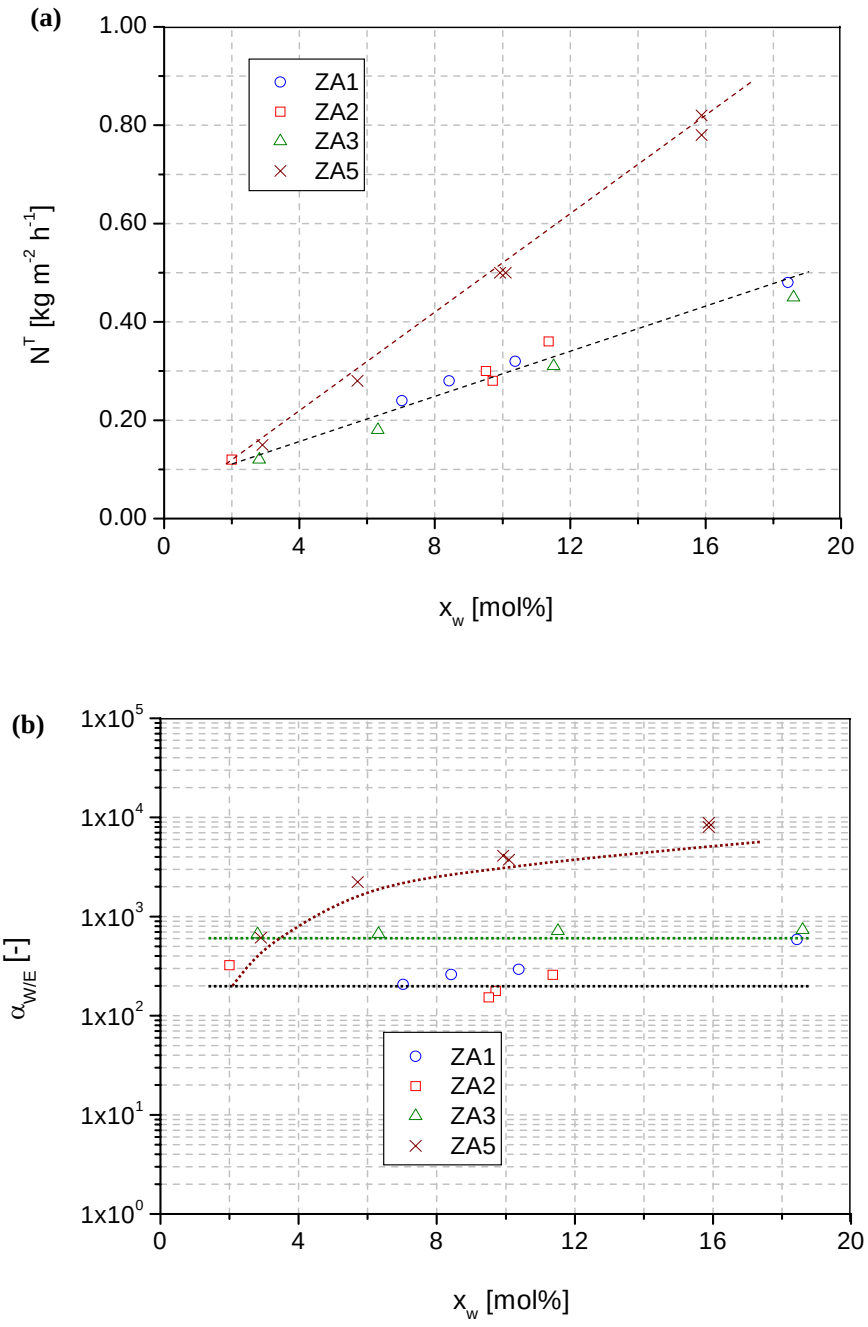

FigureV.4: Evolution of (a) total flux and (b) water/ethanol selectivity with water feed composition (molar) for membranes ZA1-ZA3 and ZA5. VPV conditions: X_w = 0-10 wt.% (x_w = 0-22 mol%), T=323 K, P_v = 1 mbar, P_o = 1.0 bar. Standard deviation ≤5% for total flux and ≤10% for selectivity. Dashed and dotted lines refer to the trends observed, respectively, for total flux and selectivity.

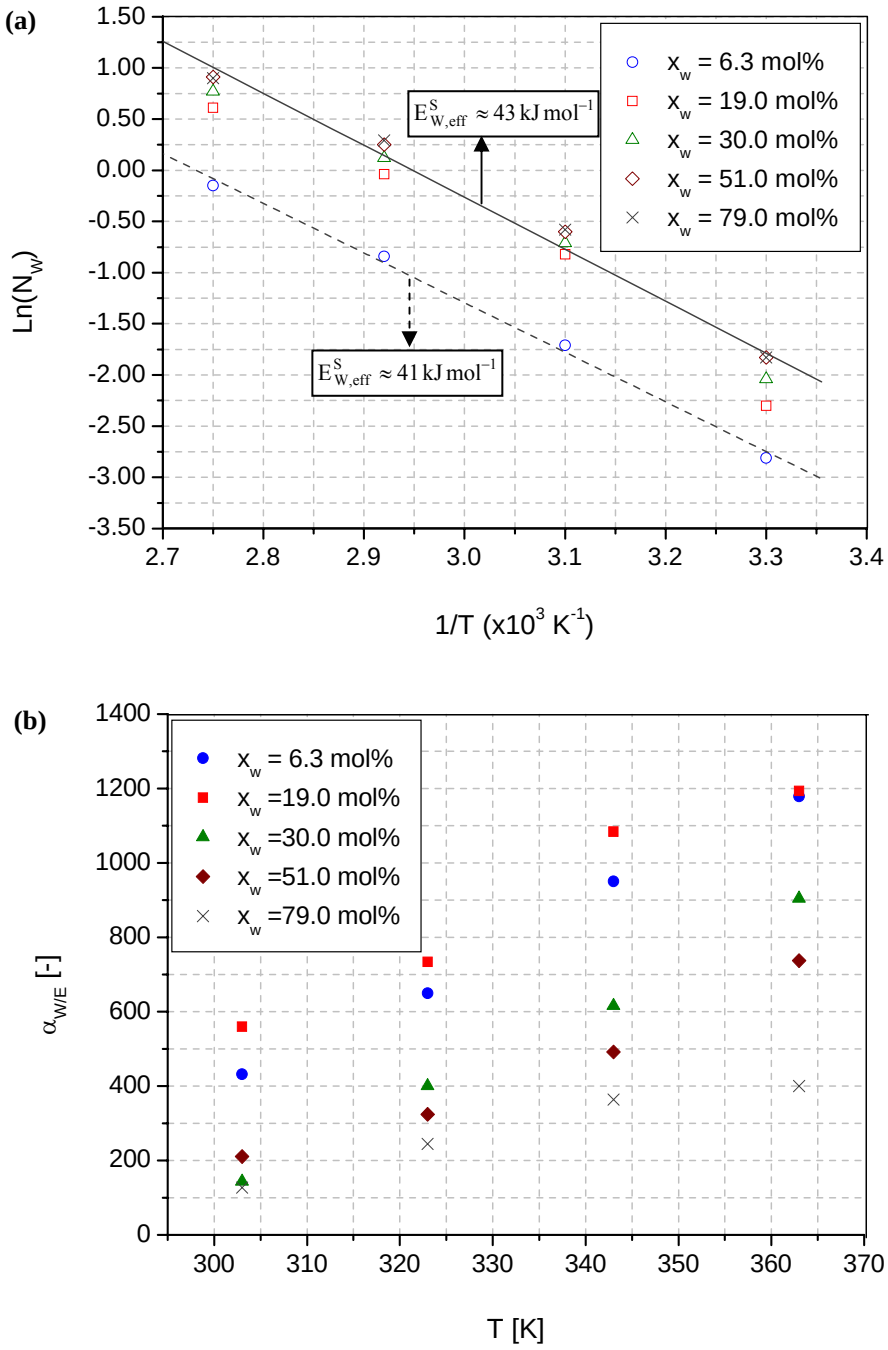

Figure V.5: Evolution of (a) total flux and (b) water/ethanol selectivity with temperature for membrane ZA3. VPV conditions: $X_w \approx$ 2.5-59 wt.% (x_w = 6.3-79.0 mol%), P_o = 1.6 bar, P_v = 1 mbar. Standard deviation ≤2% for total flux and ≤4% for selectivity. Straight and dashed lines refer to linear fittings for water flux.

Table V.3: Apparent activation energies for water flux across zeolite NaA membranes. VPV conditions: P_o =1-3 bar; P_v =1-3 mbar

Membrane	*X_w range (wt.%)*	*T range [K]*	*$E_{a,eff}$ [kJ mol^{-1}]*	*Reference*
ZA-2	4.8-5.2	303-363	40	This study
ZA-3	2.5-59.0	303-363	41-43	This study
ZA-4	4.3-4.7	303-363	34	This study
ZA-5	3.9-4.2	303-363	35	This study
Zeolite NaA (outer-side)	10-100	313-353	35	Okamoto et al. (2001)
Zeolite NaA (flat)	10	313-353	51-52	Shah et al. (2000)

than that found in the range 19-79 wt.%. This observation might be ascribed to the dramatic reduction of the water activity in the feed, thus causing a reduction of the water driving force and therefore a lowering of the water flux.

On the other hand, the water/ethanol selectivity of membrane ZA3 also tends to rise with temperature in the range 303-363 K (see Figure V.5b), namely better separations can be achieved at higher temperatures. In fact, this trend is opposite to that reported by *Okamoto et al. (2001)* for the separation of ethanol/water mixtures by VPV and by *Van den Graaf et al. (1999)* for gas separations with MFI zeolite membranes. The discrepancy between these trends might be ascribed to the presence of a reduced number of non-zeolite domains in the membranes prepared in this work. A raise of temperature might enhance water transfer through the zeolite layer, thus compensating the effect of ethanol transfer through non-zeolite pores and giving rise to a global increase of the membrane selectivity.

The trend of the total flux and water/ethanol selectivity with temperature at low water compositions (10 mol% or 5 wt.%) is more clearly plotted in Figure V.6 for membranes ZA2-ZA5. As can be seen, an Arrhenius trend of the total flux with temperature is also observed in Figure V.6a, with effective activation energies lying in the range 34-41 kJ mol^{-1} (see Table V.3). No remarkable differences in terms of effective activation energies are found for membranes prepared onto α-Al_2O_3 and TiO_2 (rutile) supports. Furthermore, a lower positive trend of selectivity with the temperature is observed for membrane ZA2 (see Figure V.6b) at low water feed fractions, but membranes ZA4 and ZA5 prepared onto TiO_2 (rutile) support show decreasing trends especially beyond 340 K.

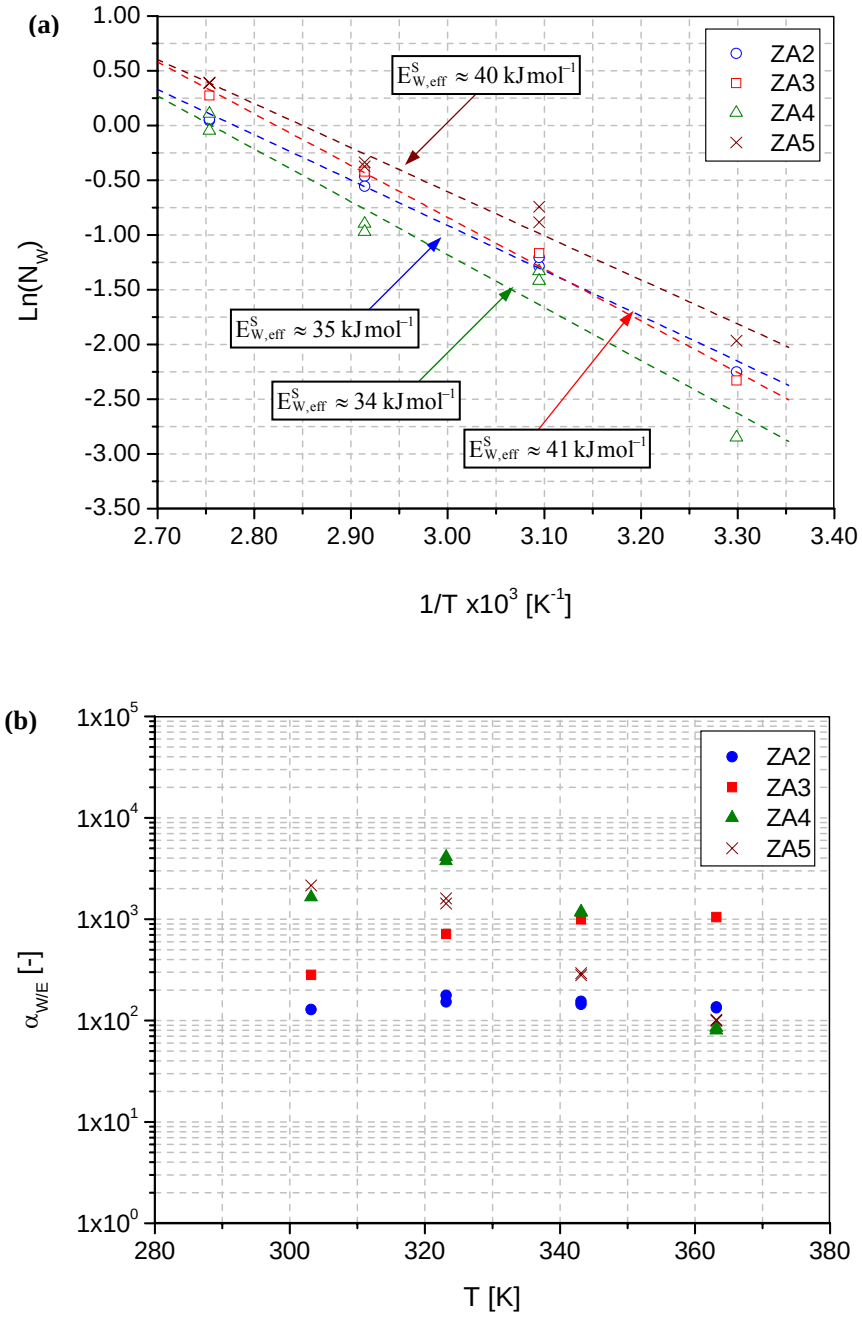

Figure V.6: Evolution of (a) total flux and (b) water/ethanol selectivity with temperature for membranes ZA2-ZA5. VPV conditions: $X_w \approx$ 0-10 wt.% (x_w = 0-22 mol%), P_o = 1.0 bar, P_v = 1 mbar. Standard deviation ≤5% for total flux and ≤10% for selectivity. Dashed and lines refer to linear fittings for water flux.

V.1.5. Trend of permeate composition with feed composition (Y_w - X_w curve)

Figure V.7 shows the effect of the water composition in the feed in the composition of the vapor permeate (Y_w - X_w curve) for membrane ZA3 in the temperature range 303-363 K. As can be seen, because water/ethanol selectivities are very high, the permeate is highly enriched with water. It should be mentioned that the composition of the permeate is >90 wt.% for feed water fractions <2-4 wt.%. The membrane is more enriched in water at higher temperatures, in agreement with the positive effect exerted by temperature to selectivity shown in Figure V.5b.

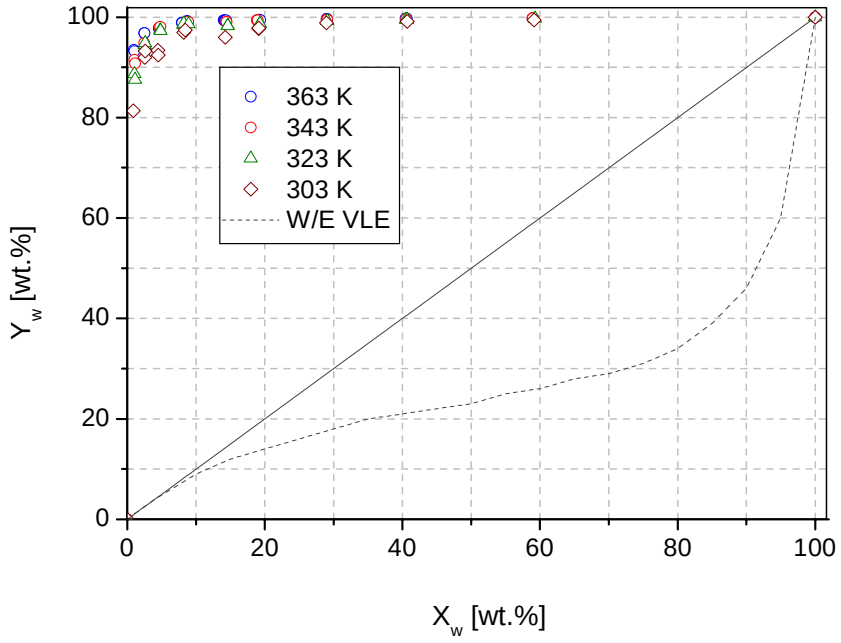

Figure V.7: Permeate composition vs. feed composition for membrane ZA3 at the temperature range 303-363 K. Experimental PV conditions as in Figure V.5. The dotted line refers to the VLE diagram for the ethanol/water mixture at a pressure of 1 bar.

A simulated VLE diagram for the ethanol/water system at a pressure of 1.0 bar (activity coefficients in the liquid phase estimated by the UNIFAC method) is also included in Figure V.7. As can be observed, a distillation process (either simple or rectification) would lead to vapors enriched with ethanol instead of water due to the higher saturation vapor pressure of the former compared to that of the latter. On the contrary, zeolite NaA membranes show the ability to separate water instead of ethanol, because, as will be shown in section VIII, the separation process is not only governed by a VLE process of the liquid feed at the

liquid/membrane surface, but also by the selective adsorption of water in the zeolite layer and diffusion of both species. It should be emphasized that, compared to the VLE diagram, the differences in the separation mechanisms between distillation and pervaporation allows zeolite NaA membranes not to show the presence of any azeotrope due to the non-ideality character of the liquid feed.

V.2. VPV PERFORMANCE TOWARDS THE DEHYDRATION OF BINARY AND TERNARY MIXTURES

This section is devoted to describing the VPV performance of zeolite NaA membranes towards the dehydration of short- and long-chain primary alcohol/water binary mixtures, where the alcohols arise from methanol to 1-pentanol. Moreover, some experimental data are also provided to illustrate the VPV performance of the membranes towards the dehydration of pentanol/water/DNPE ternary mixtures, which, as was aforementioned, is a subject of special interest for future prospects in the field of zeolite NaA membrane reactors to carry out etherification reactions with a selective removal of water. Membrane ZA2, which showed good VPV performance towards the dehydration of ethanol/water mixtures, was used to carry out the experiments described in this section. The VPV performance of membrane ZA2 towards the dehydration of the alcohol/water mixtures surveyed in this study is shown in Table V.4. Moreover, the details concerning the operational conditions tested are summarized in Table V.5.

V.2.1. Effect of the number of carbon atoms (C) of the alcohol

Figure V.8 shows the evolution of the total flux and water/alcohol selectivity with the number of carbon atoms (C) in the chain of the primary alcohols in the PV of alcohol/water binary mixtures across membrane ZA2 at the same water feed composition (molar). As can be seen, while the total flux seems to be practically independent on the nature of the alcohol in the mixture (see Figure V.8a), the selectivity appears to depend exponentially on the number of carbon atoms in the chain, with values up to 3000 in the water feed composition range 1.7-7.3 wt.% (see Figure V.8b). Table V.6 shows the total flux and water/organic selectivities reported in the literature towards the dehydration of organic mixtures by VPV with zeolite NaA membranes. As can be seen, membrane ZA2 surveyed in this work shows total fluxes and water/alcohol selectivities comparable to those listed in Table V.6 for the dehydration of long-chain alcohols and ethers.

Table V.4: VPV performance of membrane ZA2 towards the dehydration of binary and ternary alcohol mixtures. PV conditions: X_w = 4.1-5.0 wt.%; T = 323 K; P_o =3 bar; P_v =1 mbar

Mixture	Y_W *(permeate) (wt.%)*	$\alpha_{W/E}$ *[-]*	N^T *[kg m^{-2} h^{-1}]*
Methanol/water	60.43	29	0.33
Ethanol/water	92.82	258	0.36
1-propanol/water	96.44	525	0.35
1-butanol/water	97.14	778	0.39
1-pentanol/water	98.85	1905	0.38

Table V.5: Experimental conditions for VPV experiments with ethanol/water mixtures

Feed flow rate [mL min^{-1}]	300
Water feed composition (X_w) [wt.%]	1.7-7.3
Temperature (T) [K]	323-403
Feed pressure (P_o) [bar / kPa]	3.0 / 300
Permeate vapor pressure (P_v) [mbar / Pa]	1-5 / 100-500
Stabilization time [h]	2-4
Experimental time [h]	0.5-3.0
Number of replicates [-]	2-3

The aforementioned trends of total flux and alcohol/water selectivities in membrane ZA2 might be ascribed to the higher affinity that zeolite NaA shows to polar molecules due to its strong hydrophilic character. Thus, the zeolite active layer might preferentially adsorb short-chain alcohols (methanol and ethanol) over long chain alcohols (butanol and pentanol) and, as a result, the membrane would show higher water/alcohol selectivities for long-chain alcohols than for short-chain ones. However, because the polarity of water is much higher than that of the alcohols surveyed in this study, the adsorption of water on zeolite NaA is expected to be much higher and, therefore, water flux across the membrane would be almost constant for all the alcohol/water mixtures at the same feed water composition (molar). It should be noted that, according to Figure V.8a, the total flux for methanol/water mixtures seems to be lower than that of the rest of alcohol/water mixtures. This result might be accounted for by the higher similitude that water and methanol molecules show due to short carbon chain of the latter.

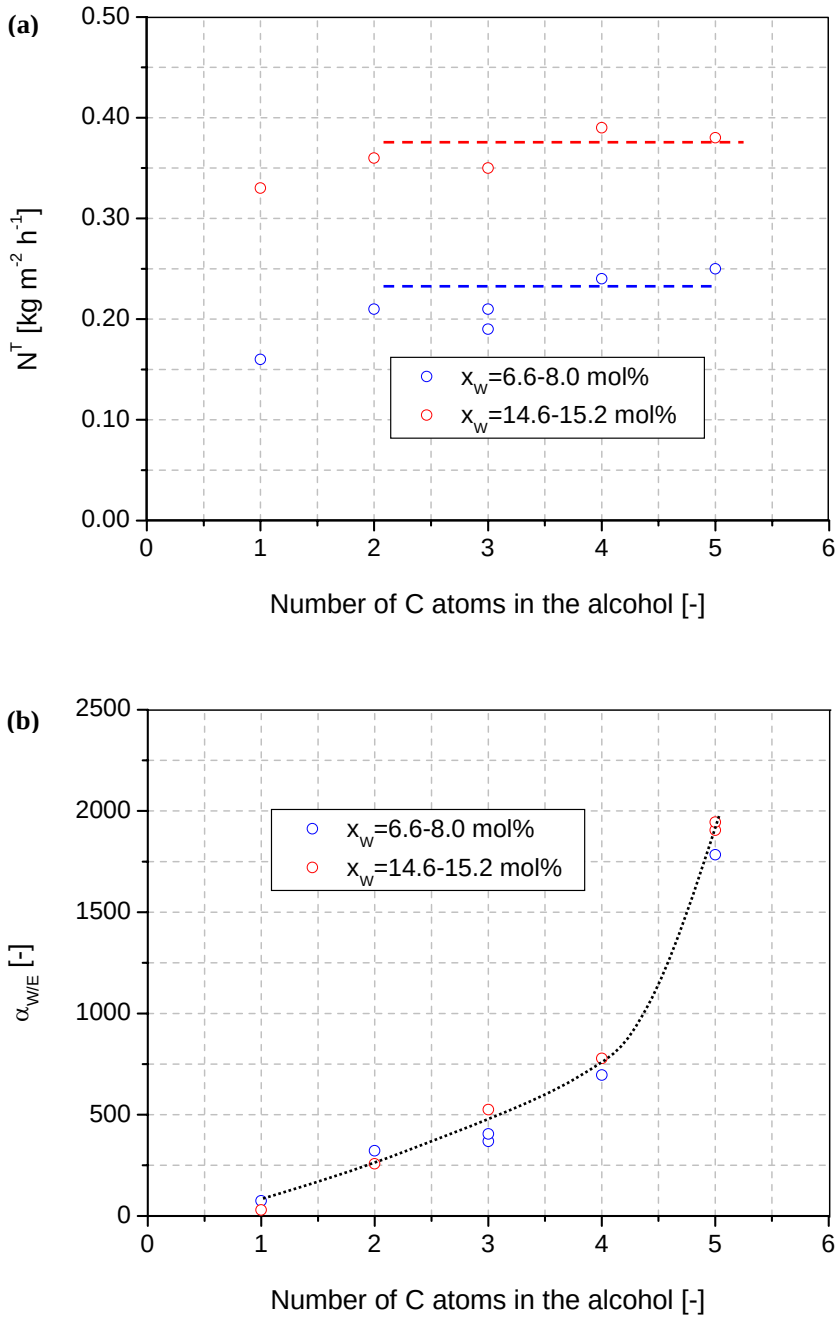

Figure V.8: Evolution of (a) total flux and (b) water/alcohol selectivity with the number of carbon atoms in the alcohol for membrane ZA2. VPV conditions: P_o = 3.0 bar, P_v = 1 mbar. Standard deviation ≤5% for total flux and ≤10% for selectivity. Dashed and dotted lines refer to the trends observed, respectively, for total flux and selectivity.

Table V.6 VPV performance of zeolite NaA membranes towards the dehydration of organic liquid mixtures

Thickness of the zeolite layer [μm]	*Support*	*Organic*	*Water in feed [wt.%]*	*T [K]*	*Flux [kg m^{-2} h^{-1}]*	*Selectivity (W/Alcohol) [-]*	*Reference*
7	TiO_2 inner tube	MeOH	6	323	0.33	29	**Pera-Titus et al. (2006b)**
		EtOH	6	323	0.36	258	**(This study)**
		1-PrOH	5	323	0.35	525	
		1-BuOH	5	323	0.39	778	
		1-PeOH	5	323	0.38	1905	
		1-PeOH/DNPE	2	323	0.25	2860	
NA	mullite tube	UDMH	5	318	0.30	>10000	Kazemimoghadam et al. (2004)
NA	Ceramic	THF	6.1	333	0.41	2000	Urtiaga et al. (2003)
NA	Ceramic	t-BuOH	10	333	1.70	16000	Gallego-Lizon et al. (2002)
30	α-Al_2O_3 outer tube	MeOH	10	323	0.58	2100	Okamoto et al. (2001)
		EtOH	10	348	2.16	10000	
		2-PrOH	10	348	1.77	10000	
		Acetone	10	323	0.90	5600	
		DMF	10	333	0.90	9000	
NA	ZrO_2 / C	2-PrOH	10	343	0.79	4000	Jafar and Budd (1997)

NA: Not available

V.2.2. Effect of the feed composition

Figure V.9 shows the effect of the feed composition at 323 K on the total flux and water/alcohol selectivities for ethanol/water and pentanol/water mixtures at low water feed compositions (<20 mol% or 8 wt.%) for the membrane ZA2 (synthesized onto α-Al_2O_3 support). As can be seen, the total flux tends to increase linearly with the water composition with the same slope for both mixtures (see Figure V.9a), while the selectivity remains practically constant (see Figure V.9b), water/1-pentanol selectivities being one order of magnitude higher than water/ethanol ones. These trends are in agreement with those reported in Figure V.4 for membranes prepared onto α-Al_2O_3 support.

V.2.3. Effect of temperature

Figures V.10 shows the effect of temperature on the water flux and water/alcohol selectivity for membrane ZA2 at low feed water compositions (<20 mol% or 8 wt.%) for the VPV dehydration of ethanol/water and 1-pentanol/water binary mixtures and 1-pentanol/ DNPE/water ternary mixtures for different feed compositions. As can be seen in Figure V.10a, water flux shows an Arrhenius trend for all the mixtures, with effective activation energies for water of 34 kJ mol^{-1} for ethanol/water mixtures and 20-24 kJ mol^{-1} for 1-pentanol/water and 1-pentanol/DNPE/water mixtures. For the latter two mixtures, irrespective of the presence of DNPE, total flux seems to depend only on feed composition.

On the other hand, the water/ethanol and water/1-pentanol selectivities are almost constant with temperature in the range 303-410 K (see Figure V.10b), being the latter one order of magnitude higher than the former, with values up to 3000, in agreement with the trends reported in Figure V.9b. Moreover, water/1-pentanol selectivities are higher for lower water feed compositions (7.8-9.5 %mol or 1.7-2.1 wt.%) than for higher (22.8-27.9 %mol or 5.7-7.3 wt.%). For the former water feed composition range, water/mixture selectivities (mixture = 1-pentanol + DNPE) show similar values as water/1-pentanol selectivities. This result confirms that hydrophobic species are not discriminated by zeolite NaA membranes, and therefore water/mixture selectivities only depend on water feed composition.

V.3. SIMULATION OF A MULTITUBULAR PV ZEOLITE NaA MEMBRANE REACTOR TO CARRY OUT THE LIQUID-PHASE ETHERIFICATION REACTION OF 1-PENTANOL TO DNPE

In light of the general trends shown in this section, good quality zeolite NaA membranes appear to be good candidates for the dehydration of organic mixtures by VPV,

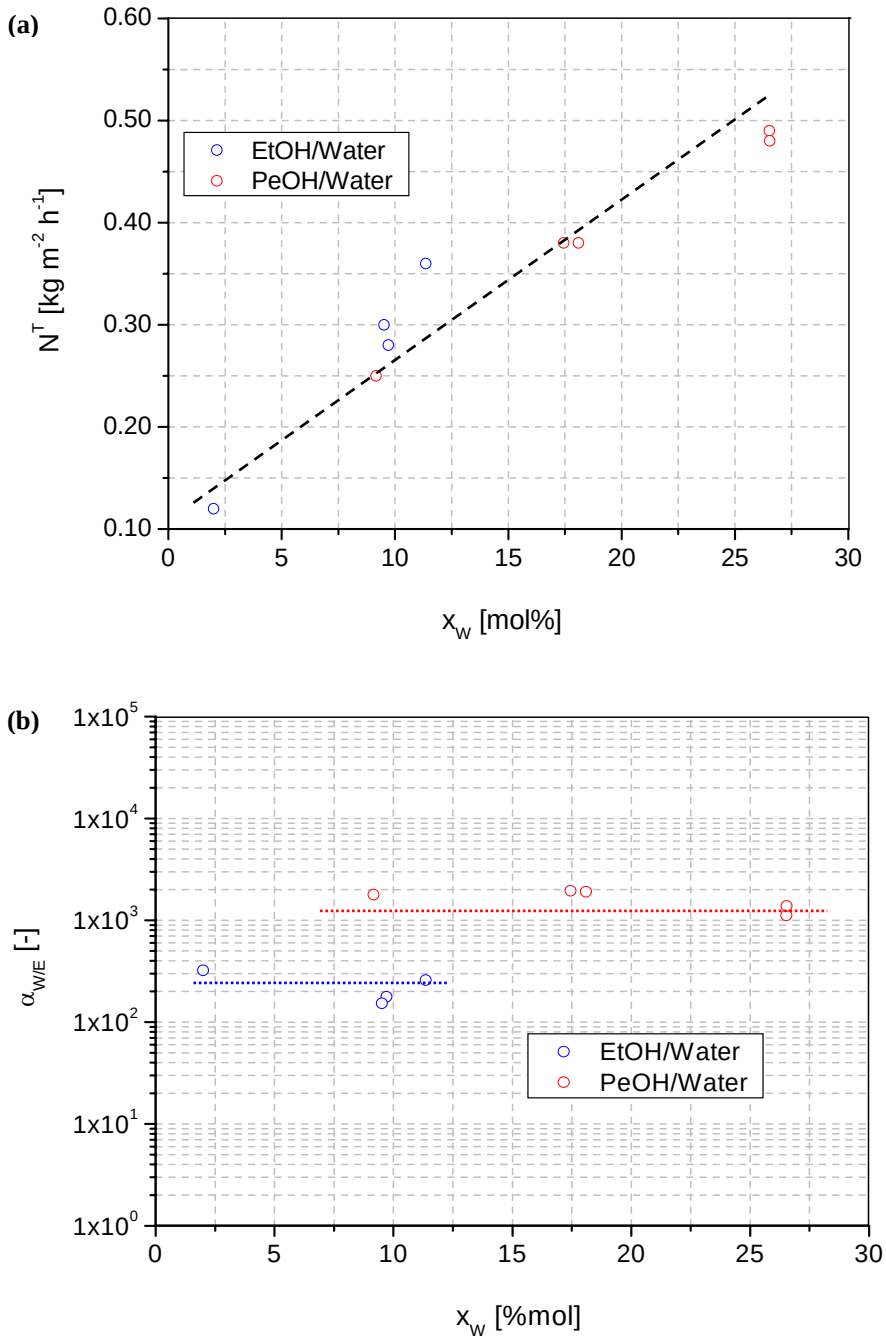

Figure V.9: Evolution of (a) total flux and (b) water/alcohol selectivity with water feed composition for membrane ZA2. VPV conditions: Xw=0-10 wt.%, T=323 K, P_o = 3.0 bar, P_v = 1. Standard deviation ≤5% for total flux and ≤10% for selectivity. Dashed and dotted lines refer to the trends observed, respectively, for total flux and selectivity.

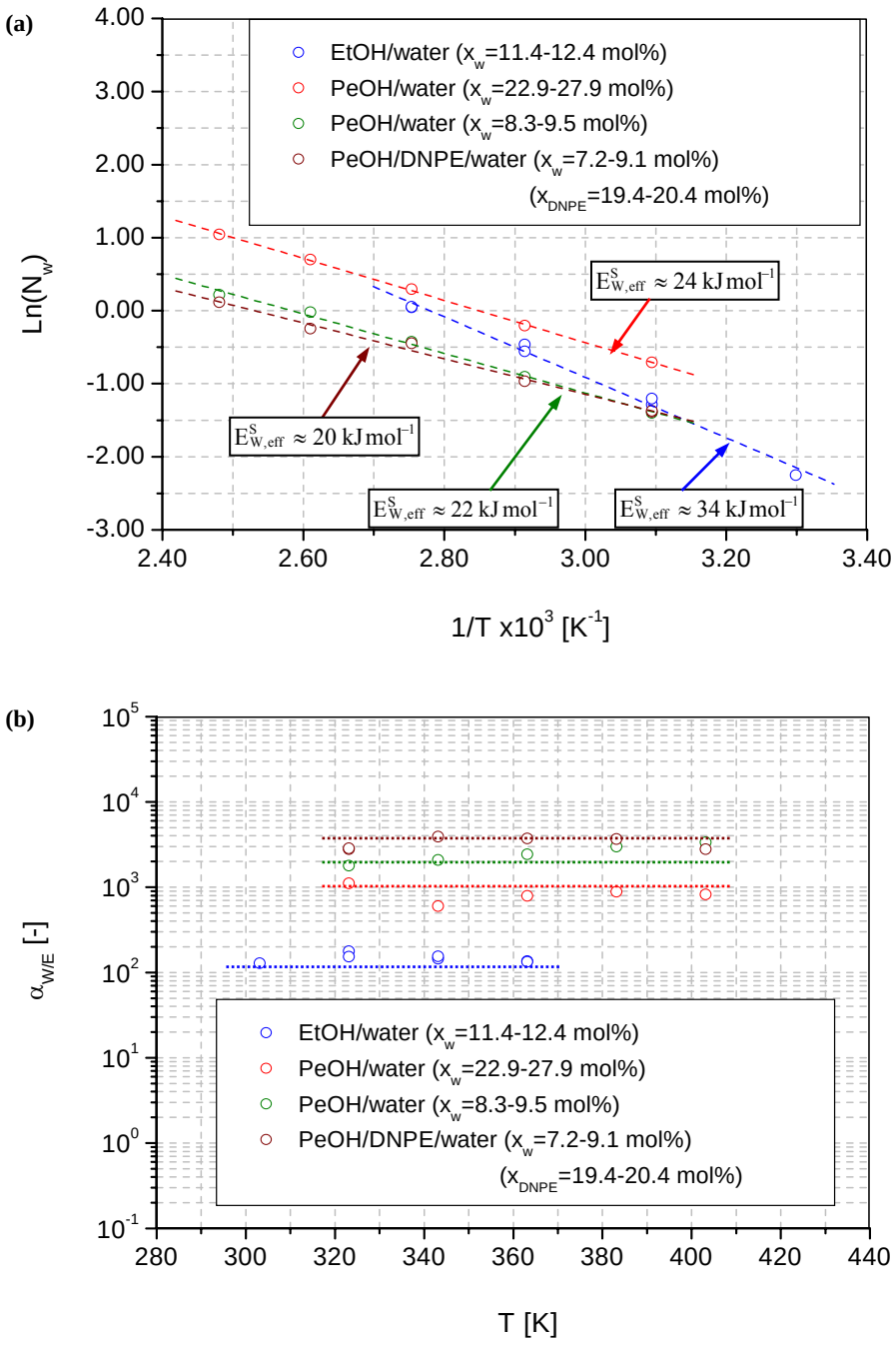

Figure V.10: Evolution of (a) total flux and (b) water/alcohol selectivity with temperature atoms in the alcohol for membrane ZA2. VPV conditions: X_w = 0-10 wt.%, P_o = 3.0 bar, P_v = 1 mbar. Standard deviation ≤5% for total flux and ≤10% for selectivity. Dashed and dotted lines refer, respectively, to linear fittings for water flux and to the trend observed for selectivity.

because they offer **high selectivities towards water removal** and **high fluxes at the same time**. High selectivities are required to remove selectively one species of a mixture instead of other valuable ones, while high total fluxes are needed to reduce the membrane area for a desired production. The strong dehydration performance of the zeolite NaA membranes synthesized in this work is especially remarkable for the dehydration of the ternary mixture 1-pentanol/water/DNPE, since the PV of DNPE across the membranes is practically negligible over a broad range of experimental conditions due to the low adsorption of long-chain alcohols and ethers in the membrane. In view of these results, zeolite NaA membranes might be also expected as promising candidates for PV zeolite membrane reactor applications in the absence of an acid environment that might dissolve zeolite NaA layers.

As was aforementioned in section I.4.1.2.2., commercial applications of zeolite membranes are desirable in high-area applications such as bundles of small-bore or capillary supports. However, these applications might suffer from high pressure drops along the modules due to friction. In this section we present some preliminary results concerning the modeling of a multitubular PV zeolite NaA membrane reactor to carry out the liquid-phase etherification reaction of 1-pentanol to DNPE catalyzed by the commercial gel-type microporus ion-exchange resin CT-224 from Purolite Co. (Bala Cynwyd, PA) with 5.34 meq H^+ (kg of dry resin)$^{-1}$ and cross linking of about 4 wt.% divinylbenzene to illustrate the enhancement of 1-pentanol conversion that can be achieved compared to a fixed-bed reactor configuration due to the selective removal of water by the membrane. The calculations have been performed from experimental membrane separation data (section V.2) and kinetic data.

V.3.1. Stoichiometry and kinetics of the reaction

For modeling purposes, the stoichiometry of the overall reaction catalyzed by CT-224 resin at 423 K taking into account the main subproducts that are usually obtained can be expressed by Eq. V.1 (*Pera-Titus., 2001*)

$$2.07\ (\text{1-pentanol}) \rightarrow \text{DNPE} + 1.06\ (H_2O) + 0.041\ (\text{pentenes}) + 0.016\ (\text{Other ethers})$$

Eq. V.1

Furthermore, the kinetics of the reaction at 423 K can be described by Eq. V.2 (*Pera-Titus, 2001*)

$$r_{DNPE} = \frac{60.21\left(a_{1-pent}^2 - \frac{a_w\, a_{DNPE}}{0.97}\right)}{\left(1 + 3.99\, a_{1-pent} + 1.12\, a_w + 0.12\, a_{DNPE}\right)}\ [\text{mol h}^{-1}\ \text{kg cat}^{-1}], \qquad \text{(Eq. V.2)}$$

where $\mathbf{a_i}$ in the activity [-] of species **i**, that is, $a_i = \gamma_i x_i$, where in its turn $\boldsymbol{\gamma_i}$ is the activity coefficient [-] for this species calculated by the UNIFAC method.

V.3.2. Modeling

The multitubular PV zeolite NaA membrane reactor modeled in this work consists of a catalyst packed in the lumen of the membrane tubes where the liquid-phase etherification reaction takes place, while the vapor permeate side of the membrane is kept under vacuum (see Figure V.11). For simplicity, the inner side of the tubes is modeled following the general criteria usually applied for fixed-bed reactors according to the general rules put forward by *Hsieh (1996),* while the permeate side of the membrane is assumed to be perfectly mixed due to the preferential removal of water by the membrane. For the lumen of the tubes, as in a fixed-bed reactor, the evolution of the relevant variables with the position is described by a mathematical function that must be found for each special case. Moreover, temperature gradients and the hydrodynamics can also make the resolution of the bed more intricate.

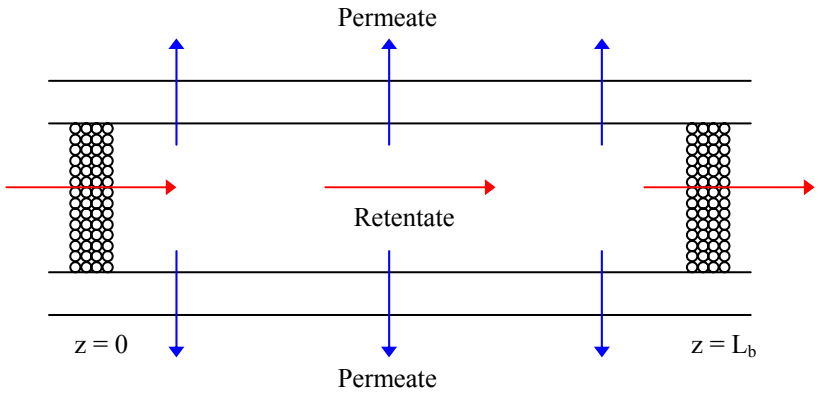

Figure V.11: Evolution of (a) total flux and (b) water/alcohol selectivity with temperature atoms in the alcohol

V.3.2.1. Flow modeling in fixed-bed reactors

In general terms, several phenomena that might occur altogether in a fixed-bed reactor have to be taken into account in the modeling of its flow model. However, the hydrodynamics are simplified if the idealized plug flow model can be assumed. The most typical effects that cause deviations from the idealized plug flow are described in the literature, as well as some criteria or well-established heuristics to assure that they are negligible or at least to reduce their contribution (*Rase, 1977*). The main effects are the following ones:

V.3.2.1.1. Velocity gradients normal to the flow direction due to wall effects

The turbulence in an empty tube tends to promote the presence of an idealized plug-flow or flat velocity profile over a cross section (see Figure V.12). The turbulence in a tube can be increased due to the presence of particles (fixed-bed reactor) and thus, a flat velocity profile can be attained at lower velocities. However, a peak velocity is usually observed at about one particle diameter from the wall (see Figure V.12b). According to *Schwartz and Smith (1953)*, the velocity profile in a fixed-bed reactor does not tend to deviate more than 20% from the flat profile when D_b/D_p >30, where $\mathbf{D_b}$ and $\mathbf{D_p}$ correspond, respectively, to the bed diameter and the mean particle size [m].

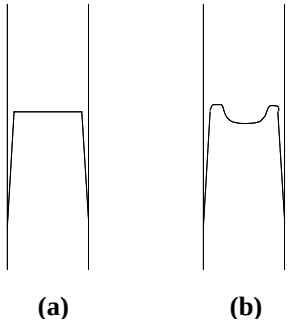

Figure V.12: Velocity profiles in tubular reactors. (a) Idealized plug-flow; (b) Flow through packing (*Rase, 1977*).

V.3.2.1.2. Axial dispersion

The axial dispersion in a fixed-bed reactor is attributed to stream splitting, acceleration, deceleration and trapping (*Rase, 1977*). The axial dispersion may be neglected for gases with Peclet Number (N_{Pe}) of 2 for a ratio $L_b/D_p \geq 100$, and for liquids with Peclet Number (N_{Pe}) of 1 for a ratio $L_b/D_p \geq 200$, where L_b is the bed length [m] (*Rase, 1977*).

V.3.2.1.3. Velocity gradients caused by poor distribution of reactants

A poor distribution of reactants over an entire cross section of a tubular reactor is a common problem of large reactors. However, in short tubular reactors, the presence of elbows or valves placed immediately upstream of the reactor, as well as changes in the diameter of the tube, tend to perturb the uniformity of the flow. This problem can be saved by a straight length of a least 10 diameters of the pipe before the reactor.

V.3.2.1.4. Radial temperature and concentration gradients

In a tubular reactor, radial mass transfer might be caused by two main effects: (1) *wall effect*, which is deterred by the action of the particles in the bed, and (2) *concentration gradients* due to a chemical reaction. This latter aspect might be remarkable for systems with a

high ratio of reaction heat to heat dissipation capacity, where a higher temperature at the center of the reactor could lead to faster reactant depletion and product generation.

V.3.2.1.5. Channeling and shortcuts

The presence of very small particles and with a high tendency to become adhesive and to stick together can lead to local variations of porosity, which cause channeling through the bed. In addition, a fraction of the particles become inaccessible to the gas stream, which might cause a decline in solid conversion. In some practical applications, this inconvenience can be overcome by mixing the reagent particles with a dilution inert agent. However, an excess of dilution could promote the formation of shortcuts and could also play a role in the distribution of catalyst particles throughout the bed (*Van den Bleek, 1969*) due to an incomplete mixture of catalyst and inert particles.

V.3.2.2. External and internal mass transfer

External and internal mass transfer (EMT and IMT, respectively) can affect the kinetics of the reaction under study. In order to discard the contribution of both physical steps, some general criteria available in the literature can be applied. For instance, the contribution of the EMT can be assessed by the *Mears criterion*, while for IMT the *Weisz criterion* is usually applied. For further details concerning both criteria, see *Levenspiel (1999)* and section VIII.1.1. Some general recipes to estimate EMT coefficients can be found in Appendix C. In the present study, the contribution of both steps can be neglected according to the calculations reported by *Pera-Titus et al. (2001)* in a fixed-bed reactor.

V.3.2.3. Modeling a zeolite NaA membrane reactor

A quasi-isothermal PV tubular membrane reactor can be modeled by a microscopic mass balance of each species both in the lumen and permeate sides of the membrane tubes. Plug-flow and perfect mixing models are assumed to take place in both zones, respectively. Moreover, the pressure drop along the inner-side of the membrane tubes can be determined by the Ergum Equation. The following set of equations is obtained at steady-state:

- Microscopic mass balance

$$-\frac{\partial\left(w^{R}\, x_i\right)}{A_b\, \partial z} - N_i\, a_m + \rho_S \left(1-\varepsilon_b\right) r_i = 0 \qquad i= 1,\ldots N \qquad \text{(Eq. V.3)}$$

- Permeation

$$-N_i\, a_m = \frac{\partial\left(w^P\, y_i\right)}{A_b\, \partial z} \quad i= 1,\ldots N \qquad \text{(Eq. V.4)}$$

- Pressure drop (Ergum equation)

$$\frac{\partial P_o}{\partial z} = 150\,\frac{(1-\varepsilon_b)^2}{\varepsilon_b^3}\,\frac{\mu_L\, u_o}{D_p^2} + 1.75\,\frac{(1-\varepsilon_b)}{\varepsilon_b^3}\,\frac{\rho_L\, u_o^2}{D_p} \qquad \text{(Eq. V.5)}$$

Boundary conditions: $z=0 \rightarrow x_i = x_i^{in},\ y_i = y_i^{in},\ P_o = P_o^{in}$

where ρ_S is the density of the catalyst [kg m^{-3}], $\mathbf{a_m}$ is the specific area of the membrane [m^2 m^{-3}], $\mathbf{A_b}$ and $\boldsymbol{\varepsilon_b}$ are the area [m^2] and porosity [-] of the bed, respectively, $\mathbf{x_i^{in}}$ and $\mathbf{y_i^{in}}$ are the molar fraction [-] of species **i** in the retentate and permeate sides of the membrane, respectively, $\mathbf{u_o}$ is the surface velocity of the liquid inside the tubes [m s^{-1}], and $\mathbf{P_o}$ is the pressure [bar] in the lumen of the tubes. It should be noted that the set of Eqs. V.3 and V.4 that describe a membrane reactor can be reduced to a fixed-bed reactor if $N_i \rightarrow 0$ for $\forall i$ and to a tubular PV module if $r_i \rightarrow 0$ for $\forall i$. The reactor model has been solved numerically by approximating derivatives to finite differences (see Appendix B1). The number of intervals (40) has been chosen to avoid any dependence of the simulation results on them. The presence of a plug-flow together with the absence of any physical step that might contribute to the kinetics of the reaction is confirmed after the simulations.

V.3.3. Simulation results

The reactor is simulated for a production of 50000 tm/year DNPE. The input data used for the modeling are summarized in Table V.7. For preventing from high pressure drop along the membrane tubes (<15% of feed pressure), the inner diameter of the bed has been chosen at a value of 50 mm. It should be noted that this value is ca. 5 times higher than that of the α-Al_2O_3 and TiO_2 support tubes used for synthesis of zeolite NaA layers reported in chapter IV. Moreover, a value of 1000 has been chosen for the water/ethanol selectivity of the membrane and the total flux has been selected at 0.50 kg m^{-2} h^{-1}, which correspond to good quality zeolite NaA membranes that can be obtained in our laboratory according to section V.2 and seem reasonable for the operational conditions inside the reactor.

The results concerning the simulation of a membrane reactor and a fixed-bed reactor with the input data from Table V.7 are shown in Figures V.13 and V.14. Figure V.13 shows the evolution of 1-pentanol conversion, $\mathbf{X_{1\text{-}pent}}$ [-], and the rate of formation of DNPE, r_{DNPE}

[mol h^{-1} kg^{-1}], with the dimensionless length of the reactor, η = **z/L** [-] for both the zeolite membrane and the fixed-bed reactor. As can be seen, the 1-pentanol conversion in a membrane reactor reaches a value of 70%, which is much higher than the value of 43% than can be obtained with a fixed-bed reactor under the same operational conditions, because the rate of formation of DNPE is much higher due to the selective removal of water from the reaction mixture. The evolution of water composition with the non-dimensional position inside the tubes for the membrane and fixed-bed reactors is plotted in Figure V.14. As can be seen, the water composition in a fixed-bed tends to increase progressively along the reactor, while in a membrane reactor it is fairly stable at a low value along the reactor (<4 mol% or 1 wt.%) due to the selective removal of water by PV through the zeolite NaA membrane.

Table V.7: Input data for reactor modeling

x^{in}_{1-pent} [-]	1.00
$x^{in}_{w} = x^{in}_{DNPE}$ [-]	0.00
T [K]	423
P^{in}_{o} [bar / kPa]	5 / 500
P_v [mbar / Pa]	<5 / <500
Residence time [g h mol^{-1}]	35
DNPE production [tm $year^{-1}$]	50000
D_b [mm]	50 (2 in)
a_m [m^2 m^{-3}]	200
u_o range (lumen) [m min^{-1}]	0.20-0.70
ε_b [-]	25%
Catalyst: Purolite CT-224	
Density [kg m^{-3}]	710
Apparent density [kg m^{-3}]	656
Surface area [m^2 g^{-1}]	0.92
D_p [μm]	750
Membrane: Zeolite NaA[2] (inner-side)	
N_w [kg m^{-2} h^{-1}]	0.50
$\alpha_{w/1\text{-pent}}$ [-]	1000

[1] From *Pera-Titus (2001)*

[2] For simplicity, DNPE and other subproducts (pentenes, and other ethers) are assumed not be separated by the membrane due to their high hydrophobic character.

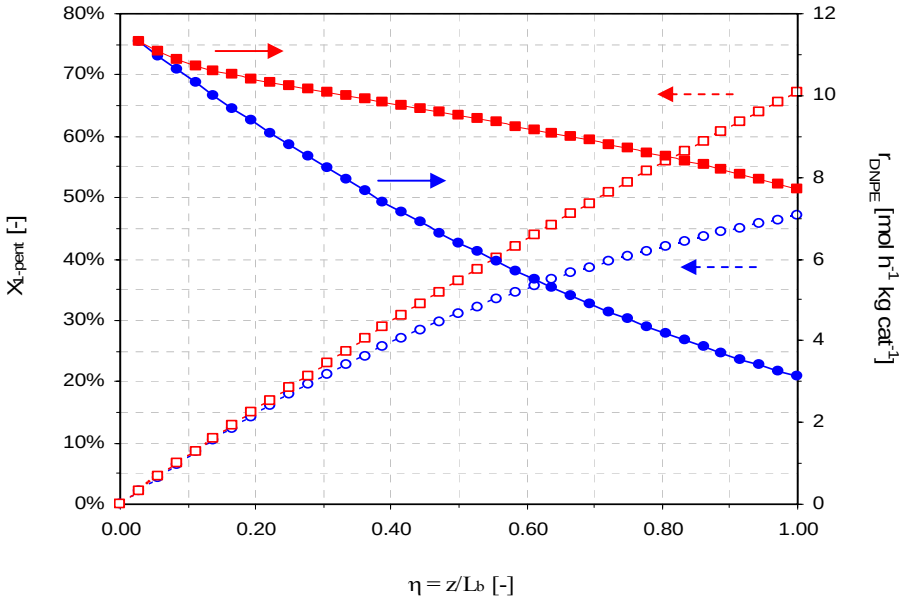

Figure V.13: Evolution of 1-pentanol conversion and rate of formation of DNPE with the position inside the reactor for fixed-bed (blue symbols) and PV zeolite NaA membrane reactor (red symbols) configurations.

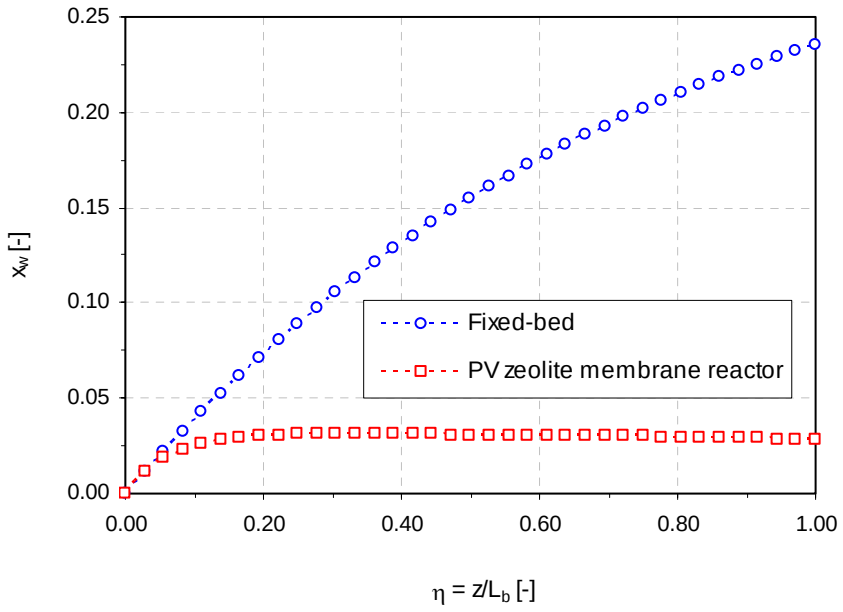

Figure V.14: Evolution of water molar fraction with the position inside the reactor for fixed-bed and PV zeolite NaA membrane reactor (red symbols) configurations.

The output data obtained from our simulations are summarized in Table V.8. As can be seen, the total length of 9 m for each tube is obtained according to the calculations. Moreover, 380 tubes of this length and 50 mm i.d. would be necessary to obtain the desired DNPE production reflected in Table V.8. Because the zeolite membrane is highly hydrophilic, *ca.* 95% of the water generated in the progress of the reaction is removed from the reaction mixture without relevant loss of the reactant, which is responsible for the enhanced 1-pentanol selectivity obtained by the reactor compared to a fixed-bed reactor operated under the same operational conditions. Finally, regarding the appropriateness of the plug-flow model in the lumen of the tubes, this model seems to describe properly the flow, since the conditions D_b/D_p >30 and L_b/D_p >200 are fulfilled, the surface velocity lies in the range $0.20 < u_o < 0.70$ m min^{-1}, and the pressure drop between the inlet and outlet of the membrane is <15% P_o.

In light of the results shown in Table V.8, the multitubular PV zeolite NaA membrane reactor might consist of bundles of 10 tubes (i.d. 50 mm, length = 1.50 m) that are envisaged to be industrially produced according to the results reported in chapter IV for inner-side tubular zeolite NaA membranes. Therefore, in a first approach, a plant to produce 50000 tm DNPE $year^{-1}$ might involve the use of at least **228** bundles (38 in parallel x 6 in series). The calculation is the following:

$$\text{No. of bundles} = 380 \text{ tubes}\,(9 \text{ m}) \times \frac{6 \text{ tubes}\,(1.5 \text{ m})}{1 \text{ tube}\,(9 \text{ m})} \times \frac{1 \text{ bundle}}{10 \text{ tubes}\,(9 \text{ m})} = 228 \text{ bundles}$$

(Eq. V.6)

Table V.8: Output data obtained from the simulations in the PV zeolite NaA membrane reactor

L_b [m]	9
Total length [m]	3420
Number of tubes for L_b [-]	380
$X_{1\text{-pent}}$ [%]	67
water removed [%]	~95
1-pentanol removed [%]	<0.05
Efficiency [tm DNPE / kg dry cat]	14.6
Hydrodynamics	
D_b/D_p [-]	67 > 30
L_b/D_p [-]	2100 > 100
Pressure drop [kPa]	16 (<15% P_o^{in})
u_o [m min^{-1}]	~0.30

V.4. DISCUSSION AND FINAL REMARKS

In view of the results obtained and discussed in sections V.1 and V.2, the zeolite NaA membranes synthesized in this work show good performance towards the dehydration of alcohol/water mixtures by VPV, the process being especially favored for long-chain alcohols. Moreover, long-chain ethers like DNPE have been found not to pervaporate through the membranes. In light of our experimental results, a PV zeolite NaA membrane reactor has been simulated in section V.3 to carry out the liquid-phase synthesis of DNPE from the etherification of 1-pentanol. According to our simulations, a plant based on 230 zeolite NaA bundles could produce 50000 tm DNPE $year^{-1}$ with a higher conversion than a conventional fixed-bed reactor due to a selective water removal by the membrane and thus a reduction of the inhibition of the catalyst. Further research is required on the one hand to improve the calculations by using improved versions of the kinetics of the reaction taking into account the swelling effect of the resin due to the polarity of the reaction mixture and on the other hand to assess experimentally the appropriateness of a zeolite NaA membrane reactor to synthesize DNPE in a similar manner as was reported by *de la Iglesia et al. (2005)*.